Research in Astronomy and Astrophysics, 23:055002 (8pp), 2023 May https://doi.org/10.1088/1674-4527/acc151

NGC 4117: A New Compton-thick AGN Revealed by Broadband X-Ray Spectral Analysis

Pavithra Mohanadas and Adlyka Annuar
Department of Applied Physics, Faculty of Science and Technology, Universiti Kebangsaan Malaysia, 43600 UKM Bangi, Selangor, Malaysia; adlyka@ukm.edu.my
Received 2022 December 14; revised 2023 February 8; accepted 2023 February 20; published 2023 April 17

Abstract

In this paper, we present the broadband (0.5–195 keV) X-ray spectral analysis for one of the newly detected AGNs in the Swift-BAT 105 month Hard X-ray Survey Catalog, NGC 4117. According to our ongoing research on low luminosity AGNs from the Swift-BAT 105 month catalog, we examine whether they are indeed low luminosity or heavily obscured AGNs. One of the AGNs in our sample is NGC 4117, where we discover it could be potentially a CTAGN. Therefore to examine NGC 4117 in detail, we combined the high energy Swift-BAT data with low energy data from XMM-Newton and Swift-XRT, and fitted the spectra simultaneously using physically-motivated models. A high absorption occurred at lower energies, i.e., below 3 keV. Past studies suggested that NGC 4117 was heavily obscured with a large column density ($\sim 10^{23}$ cm^{-2}). Our fitting suggests that this AGN is in the Compton-thick regime with a predicted line-of-sight column density ($N_{\rm H,los}$) of 3.82×10^{24} cm^{-2} and a torus column density ($N_{\rm H,tor}$) of 3.07×10^{24} cm^{-2}. Both models yield intrinsic luminosity of 1.03×10^{42} erg s^{-1} at 2–10 keV while our bolometric luminosity is 2.05×10^{43} erg s^{-1}, indicating that NGC 4117 is not an intrinsically low luminosity AGN. Rather, it is a standard AGN. The value of Eddington ratio that we obtained is 0.22, suggesting a very high accretion rate for this AGN.

Key words: galaxies: active – X-rays: galaxies – techniques: spectroscopic

1. Introduction

The compact region in an active galaxy is known as an active galactic nucleus (AGN), where a supermassive black hole fuels it by accreting materials. An accretion disk of infalling material, together with a donut-shaped torus of gas and dust at a larger scale, encloses the core supermassive black hole, as per the AGN unified model (Antonucci 1993; Urry & Padovani 1995). However, several studies have suggested that some AGNs lack an accretion disk, especially AGNs with low luminosity ($L_{\rm bol} < 10^{42}$ erg s^{-1}) according to the absence of an ultraviolet bump (e.g., Shakura & Sunyaev 1973; Macchetto & Chiaberge 2007; Eracleous et al. 2010) and broad iron Kα line at $\sim$6.4 keV (e.g., Guainazzi et al. 1996; Terashima et al. 2002; Younes et al. 2011). Mason et al. (2013) predicted that a low luminosity AGN (LLAGN) may instead hold a truncated accretion disk. Fundamentally, an LLAGN is suggested to be a weak AGN because of its slow accretion rate, in which the black hole is underfed (Panessa et al. 2006; Yuan & Narayan 2014). As accretion rate decreases, this could also cause the torus structure to gradually break down, and ultimately disappear (e.g., Elitzur & Shlosman 2006; González-Martín et al. 2017; Diaz et al. 2020).

An AGN, however, may also appear to be less luminous if it is deeply hidden from the line-of-sight by dense gas and dust clouds, particularly within the torus. For example, many observed LLAGNs have been identified to be, in fact, standard AGNs ($L_{\rm bol} \geqslant 10^{42}$ erg s^{-1}), which are heavily obscured (e.g., Imanishi et al. 2007; Ricci et al. 2016; Annuar et al. 2020; Lambrides et al. 2020). When our line-of-sight to the AGN is blocked by gas and dust, where its column density becomes higher than the Thomson scattering cross-section inversion; i.e., $N_{\rm H} \geqslant 1.5 \times 10^{24}$ cm^{-2}, the AGN is referred to as a Compton-thick AGN (CTAGN). Due to this extreme obscuration, it can be misidentified as an LLAGN. Therefore, a detailed examination of an AGN with low luminosity is essential to distinguish an intrinsic LLAGN from a heavily obscured AGN, especially a CTAGN.

So far, broadband X-ray spectroscopic analysis is the only method that is able to identify a CTAGN reliably as it allows for direct column density measurements of the obscuring materials, and can be used to detect key features of a CTAGN such as a narrow iron Kα line at $\sim$6.4 keV by an approximately $\gtrsim$1 keV equivalent width, and a flat spectrum (i.e., observed photon index, $\Gamma_{\rm obs} \lesssim 1$ keV) at $E < 10$ keV (e.g., Goulding et al. 2012; Gandhi et al. 2014; Annuar et al. 2015, 2017; Marchesi et al. 2018; Torres-Albà et al. 2021). Unfortunately, the quality of the spectra in many cases is low due to the heavy absorption suffered by the central engine. This makes them very challenging to be identified. Nevertheless, indirect methods such as a multiwavelength indicator can be used to help us identify candidates, that can be analyzed then by further deeper X-ray observations, for the purpose of determining if AGNs are in the Compton-thick regime.

Obscuration is believed to be an important phase in AGN evolution. The obscuration of an AGN is generally influenced by the accretion rate of the central engine. One of the phenomena that can trigger an extreme accretion process is galaxy merging (Treister et al. 2012). This eventually produces a more heavily obscured AGN, especially a CTAGN, which then evolves to become an unobscured AGN at the end. Therefore, it is important to study CTAGNs in order to further understand the evolution of AGNs. The fraction of CTAGNs in the universe is believed to be between 10% and 40% based on synthesis modeling of the cosmic X-ray background radiation (e.g., Ueda et al. 2014; Comastri et al. 2015). Yet so far, only ∼8% have been directly identified based on a hard-X-ray survey by the Burst Alert Telescope (BAT; e.g., Gehrels et al. 2004), on board the Neil Gehrels Swift Observatory (Swift Marchesi et al. 2018; Torres-Albà et al. 2021; Traina et al. 2021). This suggests that we are still missing a large fraction of them.

Data from high energy X-ray observations ($E > 10$ keV) have proven to be essential in unambiguously identifying CTAGNs as they allow us to detect, or at least decompose, the AGN's direct emission, which is able to pass through obscuring materials. In the Swift-BAT 105 month all-sky survey, conducted at the 14–195 keV band, a total of 1632 high energy X-ray sources were detected (Oh et al. 2018). Among these, 422 are newly detected sources which were undetected in the previous catalog, the Swift-BAT 70 month catalog (Baumgartner et al. 2013), including the nearby galaxy NGC 4117.

NGC 4117 is an edge-on (inclination angle, $\theta_i = 90°$)[1] lenticular galaxy that lies at a distance of 17.17 Mpc away from us (e.g., Verheijen & Sancisi 2001). The galaxy hosts a Seyfert 2 (Oh et al. 2018) AGN, with 14–195 keV observed luminosity of 2.75×10^{41} erg s^{-1} (Oh et al. 2018). Based on the spectral fitting of low-energy X-ray data from the Advanced Satellite for Cosmology and Astrophysics (ASCA) observations taken in 1997, the AGN was discovered to be heavily veiled with a high column density of gas and dust; i.e., $N_{\rm H} = 3.0^{+0.90}_{-1.10} \times 10^{23}$ cm^{-2} (Terashima et al. 2000). This is supported by XMM-Newton observations taken in 2010, where the column density measured is $N_{\rm H} = 5.15^{+1.39}_{-1.22} \times 10^{23}$ cm^{-2} (Nucita et al. 2017). The estimated intrinsic luminosity by Terashima et al. (2000) at 2–10 keV, however, is marginally greater as compared to that measured by Nucita et al. (2017); i.e., 1.3×10^{41} erg s^{-1} and 5.66×10^{39} erg s^{-1}, respectively. The inconsistencies are most likely due to differences in X-ray data and models employed to fit the spectra. The latter suggest a heavily obscured AGN with low luminosity. Nucita et al. (2017) also suggested that NGC 4117 ($M_{\rm gal} \approx 3.91 \times 10^9\ M_\odot$) possesses an intermediate mass black hole, $M_{\rm BH} \approx 6.91 \times 10^5\ M_\odot$, with an accretion efficiency of 9.7×10^{-5}, indicating a low accretion rate.

The recent detection of NGC 4117 by Swift-BAT means that a broadband spectral analysis for the source is now possible. In this paper, we will specifically examine the column density of obscuring materials for NGC 4117 by performing a broadband X-ray spectral fitting, and identify the source's real nature; i.e., intrinsically low luminosity, heavily obscured AGN, or both. This source is part of our work on low luminosity Swift-BAT AGNs in an effort to characterize their broadband X-ray spectra, and uncover their true nature (Mohanadas et al. in preparation). First, we detail the data recorded from X-ray telescopes for this research in Section 2, as well as the methodology of data reduction. Then, we explain our X-ray spectral modeling approach, and present our results in Section 3. Finally, through Section 4, we analyze our findings and draw a conclusion.

2. Observations and Data Reduction

We used archival low energy X-ray data for NGC 4117 obtained by XMM-Newton (Section 2.1) and Swift X-ray Telescope (Swift-XRT) (Section 2.2), as well as high energy X-ray data taken by Swift-BAT[2] in this work. Table 1 details the log of observations used. We combined the data together with the aim of conducting broadband X-ray spectral fitting of NGC 4117 for the first time. The optical position of NGC 4117, i.e., R.A. = 12:07:46.113 and decl. = +43:07:34.87 (Oyaizu et al. 2008), is referred to in this work to extract spectra for the low energy data.

2.1. XMM-Newton

NGC 4117 was observed two times in 2010, on May 7th and November 11th by XMM-Newton with on source exposure times of 25.7 ks and 17.0 ks, respectively. The data were downloaded from the High Energy Astrophysics Science Archive Research Center (HEASARC).[3] First, we calibrated the EPIC event lists from ODF to generate spectra for the PN camera by performing EPPROC, while for the MOS camera, we used the EMPROC task. We then obtained light curves using the EVSELECT task to observe times of strong background flare activity from the EPIC event list, and created a GTI file (rate <0.4 for PN, and rate <0.35 for MOS) employing the TABGTIGEN task. The EVSELECT task was then applied to extract spectra out of a 30″ circular region with the AGN at the center as our source spectra together with the spectra out of a larger circular source free region (40″), close to the AGN as our background spectra. Subsequently, we carried out the RMFGEN task to obtain the redistribution matrix files as well as ARFGEN task for ancillary files. We then executed the SPECGROUP task

[1] The HyperLeda website (http://leda.univ-lyon1.fr/) is used as the source to obtain the host galaxy's inclination angle.

[2] The Swift-BAT 105 month catalog (Oh et al. 2018) is the source where the Swift-BAT spectrum was downloaded.

[3] https://heasarc.gsfc.nasa.gov/cgi-bin/W3Browse/w3browse.pl

Table 1
Information on the X-Ray Data for NGC 4117

Instrument (1)	ObsID (2)	Obs Date (3)	Energy Band (keV) (4)	Exposure Time (ks) (5)	Net Count Rate (10^{-3} cts s^{-1}) (6)
XMM-Newton PN, MOS1+2	0 655 800 101	2010 May 7	0.5–10	2.2, 4.9	32.4, 13.7
XMM-Newton PN, MOS1+2	0 655 800 501	2010 Nov 11	0.5–10	2.0, 8.8	2.8, 4.9
Swift-BAT	...	2004–2013	14–195	11 400	0.02
Swift-XRT	00 049 888 001	2014 Oct 3	0.5–10	8.8	2.2
Swift-XRT	00 014 105 001	2021 Mar 3	0.5–10	2.5	2.4

Note. Column (1) gives a list of instruments, column (2) provides identification number of observation (obsID), column (3) states observation date, column (4) reports energy band, column (5) provides clean exposure time of respective observation and column (6) lists the net count rate of spectrum from Swift-XRT and XMM-Newton, PN and MOS separately.

to link the associated files, and rebin the spectra to 20 counts per bin.

We checked for any evidence of variability between the two XMM-Newton observations by modeling the spectra through a simple POWERLAW model. The MOS and PN spectra of the two observations were compared separately. Both the photon index and the flux values obtained from both observations for MOS spectra are consistent within error values, where the photon index was approximately 1.46 and the flux value was 1.19×10^{-13} erg cm^{-2} s^{-1}. These showed that both observations had no significant variability, therefore we combined the MOS spectra by performing EPICSPECCOMBINE. Then, we continued with PN spectra. At first, we were unable to constrain the error values for the fit of the PN spectrum from 0655800501 obsID. Therefore, we fixed the photon index to 1.80 (Ricci et al. 2017a) for the PN spectrum from both observations. Eventually, we found no significant flux variances, indicating no variability between the two observations, thus the PN spectra were combined. Figure 1 shows the combined RGB image of NGC 4117 captured by XMM-Newton.

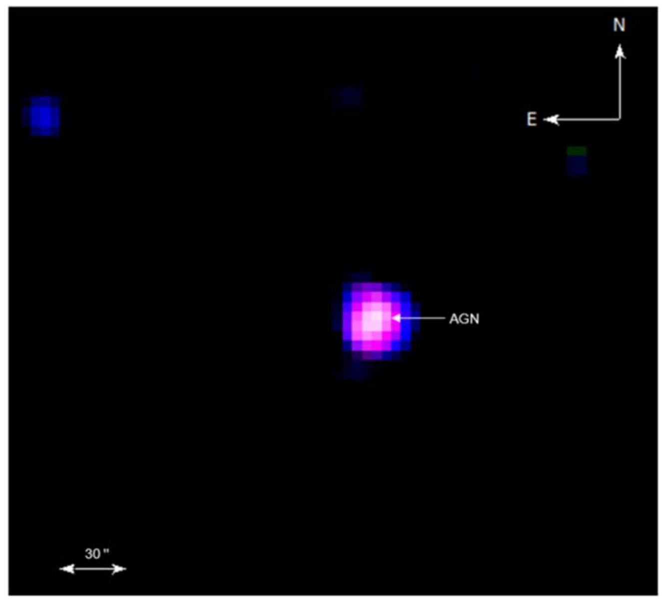

Figure 1. XMM-Newton RGB image of NGC 4117 (Red: 0.5–1 keV, Green: 1–2 keV, Blue: 2–10 keV) after combining PN and MOS event files from the two observations and smoothed with a Gaussian function.

2.2. Swift-XRT

There have been no direct observations of NGC 4117 by Swift-XRT. However, there were 16 observations of a nearby galaxy, NGC 4111, in which NGC 4117 is within the field of view in just three observations. We therefore retrieved the data for these observations. The most recent observation was taken in 2021, with an on source exposure time of 2.51 ks, while the other two observations were taken in 2014 and 2009, with on source exposure times of 0.88 ks and 2.44 ks, respectively (see Table 1).

The event file of PC mode is used for the XSELECT task in order to extract the spectra out of a 30″ circular region with AGN at the center as our source spectra, so that it matches the XMM-Newton spectra. Using the same task, the spectra were extracted out of a larger circular source free region (40″), close to the AGN as our background spectra. The ancillary files were created using XRTMKARF, and the redistribution matrix file was obtained from HEASARC's calibration database (CALDB) as ready-made files. The source spectrum was linked with its background spectrum, ancillary file and redistribution matrix file by performing the CHKEY task within GRPPHA. The resultant spectral count for one of the observations, however (ObsID 00031338007 taken in 2009), was found to have no count rate. Therefore, the observation was excluded from our analysis.

The spectral variability between the two remaining observations was examined via a simple POWERLAW model using the WebPIMMS[4] interface. The photon index was set to an AGN's typical value, which is 1.80 (Ricci et al. 2017a). According to

[4] https://heasarc.gsfc.nasa.gov/cgi-bin/Tools/w3pimms/w3pimms.pl

the simulation, we obtained approximately similar flux values for both observations, indicating no significant variability. Thus, we combined the spectra from the two Swift-XRT observations together. Due to lack of count (i.e., three counts), the spectrum was binned to 1 count per bin using GRPPHA.

3. X-Ray Spectral Fitting

We fitted the broadband spectra of NGC 4117, covering energy band from 0.5 to 195 keV by combining data from XMM-Newton, Swift-XRT and Swift-BAT. The spectral fitting was conducted using physically-motivated AGN models by Murphy & Yaqoob (2009) (MYTorus model) and Baloković et al. (2018) (borus02 model). The broadband spectra were fitted utilizing the XSPEC software (v12.11.1, Arnaud 1996). For all fits, we fixed the Galactic absorption to $N_{\rm H}^{\rm Gal} = 1.32 \times 10^{20}\,{\rm cm}^{-2}$ (Kalberla et al. 2005), as well as the redshift to $z = 0.00312$ (Verheijen & Sancisi 2001).

3.1. Basic Characterization

We began our analysis with basic characterization of the individual spectra from the three different telescopes for the purpose of investigating any variability among the observations. The spectra were modeled using a powerlaw model (zpowerlw), Galactic absorption and intrinsic AGN absorption (phabs and tbabs, respectively). In addition, we also included the zphabs × cabs × zpowerlw components to simulate Compton scattering. These components were linked to the intrinsic absorption components. The model sequence in XSPEC was as follows:

$$\begin{aligned}\text{BasicModel} &= \text{phabs}[1]\\ &\times (\text{tbabs}[2] \times \text{zpowerlw}[3]\\ &+\text{zphabs}[4] \times \text{cabs}[5] \times \text{zpowerlw}[6]).\end{aligned} \tag{1}$$

Based on our fittings, we found that all spectral parameters measured by the model for the three different spectra, such as column densities, photon indices and fluxes, were comparable to each other, manifesting no significant variability. Overall, we observed a flat photon index as well as no iron line detection in the spectra of the AGN. Together with that, the measured values of column density were on the order of $10^{23}\,{\rm cm}^{-2}$, suggesting heavy obscuration toward the AGN.

We then continued with analysis of all spectra from XMM-Newton, Swift-XRT and Swift-BAT fitted simultaneously using the same basic model (Equation (1)). An additional component, a constant, was incorporated to the model, to account for the cross-calibration uncertainties between different X-ray spectra (Madsen et al. 2015). Yet the fit was bad with χ^2/degrees of freedom (dof) of 43/17. Then, to simulate thermal emission from a hot interstellar medium at low energy, we included a component, apec. We managed to obtain a decent fit using this model with $\chi^2/{\rm dof} = 21/15$. We also tried to add a Gaussian component, ZGAUSS, to simulate potential Fe Kα emission at ∼6.4 keV, however the fit ($\chi^2/{\rm dof} = 21/14$) did not improve the model significantly (F-test probability = 1.00). Our best-fit basic model measured a column density of $1.38^{+0.68}_{-0.71} \times 10^{24}\,{\rm cm}^{-2}$, indicating a strongly obscured AGN, possibly Compton-thick. The intrinsic photon index measured is $\Gamma = 1.60^{+0.61}_{-0.61}$, compatible with an AGN's typical value (Ricci et al. 2017a). The apec component measured the plasma temperature of $0.69^{+0.19}_{-0.34}$ keV. We proceeded with our analysis of the broadband X-ray spectral fits with more complex physically-motivated AGN models, in order to obtain more reliable results for NGC 4117.

3.2. MYTorus

The MYTorus model with a toroidal reprocessor was first introduced by Murphy & Yaqoob (2009) specifically to fit the active galaxies' X-ray spectra. This model is applicable for column densities between 10^{22} and $10^{25}\,{\rm cm}^{-2}$, covering the entire regime of AGNs from Compton-thin to Compton-thick.

This model is composed of three main distinct components. The first component is a zeroth-order continuum generated by continuum photons that escaped the torus without interacting with it (MYTZ). This component is purely a line-of-sight continuum, where the intrinsic X-ray continuum is examined after the absorption resulting from the torus. The second component of the model is comprised of a scattered continuum produced from the incident photons that interacted with a reprocessed medium through Compton scattering or absorption (MYTS). It is also sometimes known as a reflection continuum when the escaping photons scatter back toward the observer. The third component is the zeroth-order (or unscattered) fluorescent emission lines generated by the absorption of a continuum photon above the K-edge threshold (MYTL).

All three components have been incorporated into our analysis. Corresponding to the respective weights of the MYTorus components, we included constants[7, 9] and fixed them to unity (Yaqoob 2012). Together with that, we also included AGNs scattering factor and its scattered power-law as specified by constant[3] and zpowerlw[4], respectively. Then, the cross-calibration uncertainties in data between the three different X-ray telescopes are accounted for using the constant [1] parameter, where we fixed the parameter to Madsen et al. (2015)'s determined value. Finally, our MYTorus model's sequence is described in XSPEC as follows:

$$\begin{aligned}\text{MYTorus} &= \text{constant}[1] \times \text{phabs}[2]\\ &\times (\text{constant}[3] \times \text{zpowerlw}[4]\\ &+ \text{zpowerlw}[5] \times \text{MYTZ}[6]\\ &+ \text{constant}[7] \times \text{MYTS}[8]\\ &+ \text{constant}[9] \times \text{MYTL}[10].\end{aligned} \tag{2}$$

First of all we coupled all MYTS and MYTL parameters to MYTZ, and fixed the inclination angle, $\theta_{\rm inc}$, to edge-on observing angle, i.e., 90°, in order to simplify the modeling.

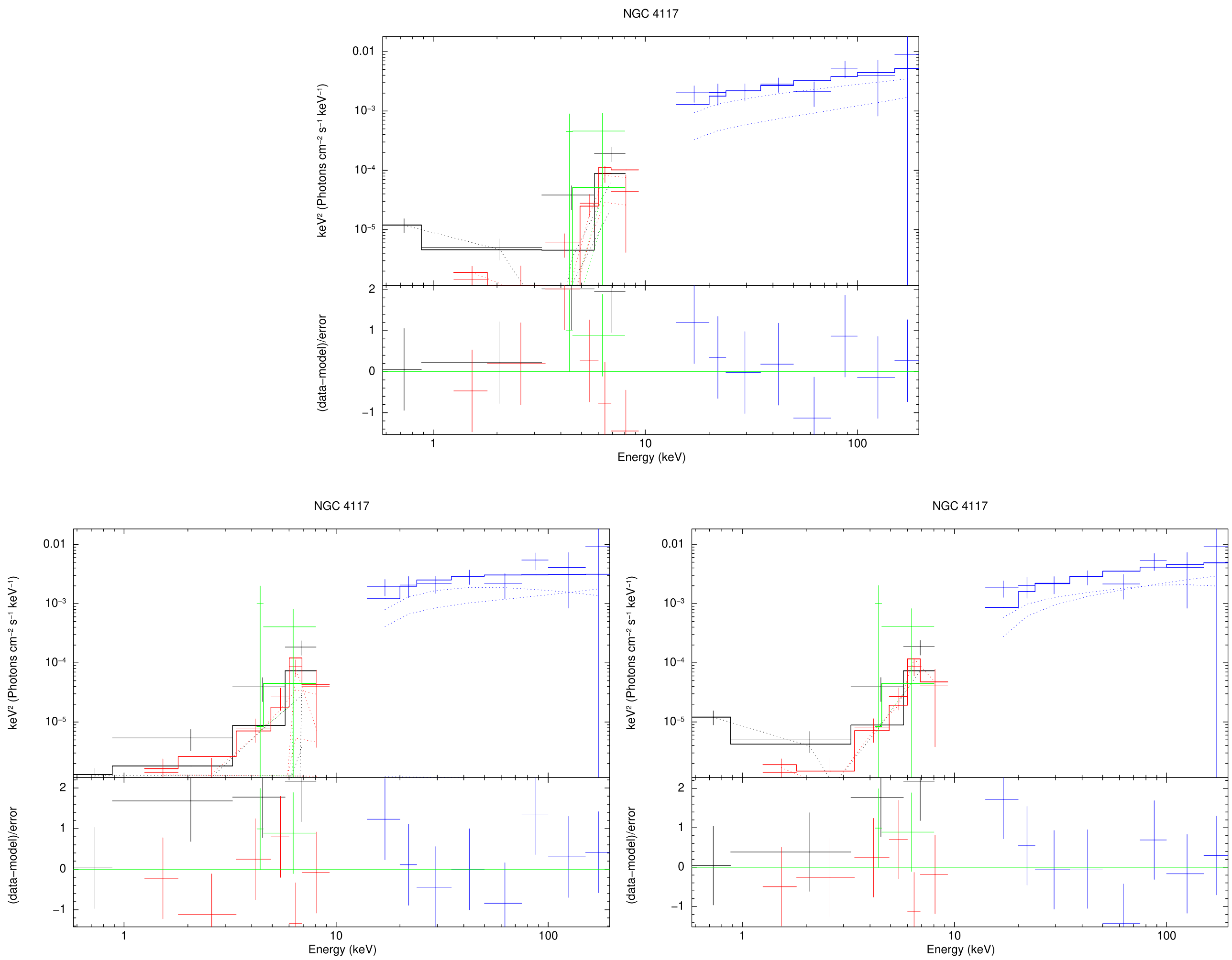

Figure 2. The best-fitted spectra from XMM-Newton PN (black), XMM-Newton MOS (red), Swift-XRT (green) and Swift-BAT (blue) using Basic Model (top), MYTorus (bottom left) and borus02 (bottom right) models.

The model yielded a decent fit with $\chi^2/\mathrm{dof} = 23/16$. However, we could not constrain the spectral parameters. We therefore tried to improve the fit by setting $\theta_{\rm inc}$ free to vary. We managed to obtain a slightly better fit with χ^2/dof of 21/15. The measured column density is $N_{\rm H,tor} = 3.01^{+4.45}_{-0.73} \times 10^{24}\,\mathrm{cm}^{-2}$ and $N_{\rm H,los} = 2.96^{+4.38}_{-0.72} \times 10^{24}\,\mathrm{cm}^{-2}$, very much in line with the Compton-thick regime. The photon index value obtained is $\Gamma = 2.03^{+0.11}_{-0.23}$, in line with an AGN's typical value (Ricci et al. 2017a). Whereas, the torus inclination angle measured is $\theta_{\rm inc} = 84.83^{+u}_{-2.48}$, indicating an edge-on orientation. The 2–10 keV observed luminosity measured is $1.46 \times 10^{39}\,\mathrm{erg\,s^{-1}}$ and the intrinsic luminosity is $5.05 \times 10^{41}\,\mathrm{erg\,s^{-1}}$. Adding an apec component to the model to account for thermal emission did not make any significant improvement to the fit. In Figure 2, we present our best-fit model and in Table 2, we tabulate its parameter values.

3.3. Borus02

The borus02 model (Baloković et al. 2018) simulates reprocessed continuum from the propagation of photons across a neutral, cold and motionless medium. This model is valid for column densities between 10^{22} and $10^{25.5}\,\mathrm{cm}^{-2}$ and it assumes the reprocessing medium to be a sphere-shape having bi-conical cutouts, corresponding to a different covering factor for a torus. Meanwhile, the torus's covering factor, $C_{\rm tor}$, is basically linked to its half-opening angle, $\theta_{\rm tor}$, that is calculated from the very center of the AGN. Therefore, this model assumes the $C_{\rm tor}$ is equal to $\cos\theta_{\rm tor}$. In addition, this model also assumes that gas is distributed uniformly, with elemental abundances of the Sun while, the iron abundance is a variable parameter.

The only spectral component in the borus02 tables is the component resulting from reprocessing in the torus. However

Table 2
X-Ray Spectral Fitting Results for NGC 4117

Parameter	Unit	MYTorus	borus02
Red χ^2	...	1.39	1.34
χ^2/dof	...	21/15	18/13
kT	keV	...	$0.66^{+0.20}_{-0.64}$
Γ	...	$2.03^{+0.12}_{-0.24}$	1.80_f
$N_{\rm H,tor}$	10^{24} cm^{-2}	$3.01^{+4.67}_{-0.75}$	$3.13^{+6.53}_{-1.95}$
$N_{\rm H,los}$	10^{24} cm^{-2}	$2.92^{+4.52}_{-0.73}$	$4.71^{+1.53}_{-3.12}$
$E_{\rm cut}$	keV	...	$300_{\rm f}$
$\theta_{\rm inc}$	deg	$84.83^{+u}_{-2.53}$	$87_{\rm f}$
$CF_{\rm tor}$	...	...	0.10^{+u}_{-u}
$f_{\rm scatt}$	...	$1.33^{+0.0002}_{-0.0001} \times 10^{-4}$	$1.07^{+0.0004}_{-u} \times 10^{-20}$
$F_{0.5-2,\rm obs}$	erg cm^{-2} s^{-1}	3.24×10^{-15}	1.49×10^{-14}
$F_{2-10,\rm obs}$	erg cm^{-2} s^{-1}	7.03×10^{-14}	1.02×10^{-13}
$F_{0.5-195,\rm obs}$	erg cm^{-2} s^{-1}	3.01×10^{-12}	3.48×10^{-12}
$F_{0.5-2,\rm int}$	erg cm^{-2} s^{-1}	2.21×10^{-11}	4.73×10^{-11}
$F_{2-10,\rm int}$	erg cm^{-2} s^{-1}	2.43×10^{-11}	7.43×10^{-11}
$F_{0.5-195,\rm int}$	erg cm^{-2} s^{-1}	4.80×10^{-11}	1.56×10^{-10}
$L_{0.5-2,\rm obs}$	erg s^{-1}	6.73×10^{37}	3.09×10^{38}
$L_{2-10,\rm obs}$	erg s^{-1}	1.46×10^{39}	2.12×10^{39}
$L_{0.5-195,\rm obs}$	erg s^{-1}	6.25×10^{40}	7.23×10^{40}
$L_{0.5-2,\rm int}$	erg s^{-1}	4.58×10^{41}	9.82×10^{41}
$L_{2-10,\rm int}$	erg s^{-1}	5.05×10^{41}	1.54×10^{42}
$L_{0.5-195,\rm int}$	erg s^{-1}	9.96×10^{41}	3.24×10^{42}
$\lambda_{\rm Edd}$	...	0.11	0.32

Note. Red χ^2 represents the reduced chi-square values and χ^2/dof represents χ^2 over degrees of freedom. kT signifies the plasma temperature. Photon index of the power-law is represented by Γ. $N_{\rm H,tor}$ is the equatorial torus hydrogen column density, while $N_{\rm H,los}$ is the line-of-sight torus hydrogen column density. $E_{\rm cut}$ is the energy cutoff. $f_{\rm scatt}$ is scattering factor and $A_{\rm Fe}$ is the iron abundance. F represents the observed (obs) or intrinsic (int) flux values at different energy bands. The intrinsic flux values were obtained by assuming no obscuration toward the AGN. L is the observed (obs) or intrinsic (int) luminosity values at different energy bands while $\lambda_{\rm Edd}$ represents the Eddington ratio. The unconstrained parameter is denoted by "u" while "f" is the fixed parameter.

in the geometry suggested for this model, there is a step function in the transmitted line-of-sight component, which is the angular function and it measures the $N_{\rm H,los}$ value. Since borus02 has only one component (borus02[4]), an absorbed line-of-sight component (available in XSPEC) was added to it via zphabs[5] and cabs[6] components. In addition, the intrinsic continuum of AGN was incorporated, as cutoffpl[7, 9] together with the scattering factor (constant[8]) of the AGN intrinsic continuum. Then, considering the cross-calibration uncertainties among data from different X-ray telescopes, we included constant[1]. Finally, the following is the sequence of borus02 model in XSPEC:

$$\begin{aligned} \text{borus02} = &\ \text{constant[1]} \times \text{phabs[2]} \\ &\times (\text{apec[3]} + \text{borus02[4]} + \text{zphabs[5]} \\ &\times \text{cabs[6]} \times \text{cutoffpl[7]} \\ &+ \text{constant[8]} \times \text{cutoffpl[9]}). \end{aligned} \tag{3}$$

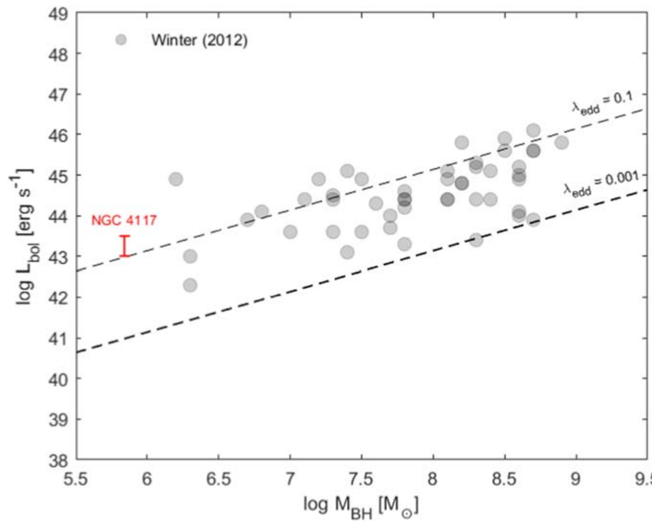

Figure 3. The plot of bolometric luminosity vs. black hole mass for NGC 4117, together with the local Swift-BAT AGNs ($z < 0.03$) from Koss et al. (2017). The red marker indicates the calculated bolometric luminosity range from our X-ray analysis for NGC 4117, and the Swift-BAT AGNs are marked in gray. The two labeled dashed lines represent the constant Eddington ratios ($\lambda_{\rm Edd} = 0.1$ and 0.001).

Initially, we linked the cutoffpl parameters to the respective borus02 parameters. All of the borus02 parameters were set free to vary, except for cos $\theta_{\rm tor}$, which was set to 0.04999 ($\theta_{\rm inc} = 87°$) to simulate an edge-on angle, and iron abundance to solar abundance; i.e., 1. This yielded a poor fit with χ^2/dof of 29/14. We attempted to improve the model by setting cos $\theta_{\rm tor}$ and iron abundance free to vary. However, we still could not obtain a good fit. Then, we tried to add an apec component to simulate thermal emission at low energy. The fit improved significantly with $\chi^2/\text{dof} = 17/12$, where it measured plasma temperature of $0.54^{+0.29}_{-0.33}$ keV. Nevertheless, the photon index reached the minimum value allowed by the borus02 model, and was therefore unconstrained. Hence, we fixed the value to 1.80 (Ricci et al. 2017a). This slightly improved the fit with $\chi^2/\text{dof} = 18/13$, which is slightly better than that obtained for the MYTorus model.

Our best-fit model measured the column densities of $N_{\rm H,tor} = 3.13^{+6.53}_{-1.95} \times 10^{24}$ cm^{-2} and $N_{\rm H,los} = 4.71^{+1.53}_{-3.12} \times 10^{24}$ cm^{-2}, consistent with being Compton-thick and in agreement with that measured by the MYTorus model. However, in 2–10 keV the observed luminosity is 1.42×10^{39} erg s^{-1}, while the intrinsic luminosity is 1.54×10^{42} erg s^{-1}, which is slightly higher than that measured by the MYTorus model. This discrepancy could be due to the different torus geometries simulated by the two models. The parameters measured by our best-fit borus02 model are also presented in Table 2, while in Figure 2, the fitted spectra are shown.

4. Discussion and Conclusion

In this paper, we have analyzed one of the newly detected Swift-BAT AGNs in NGC 4117 through a broadband X-ray spectral study, using archival data obtained by XMM-Newton, Swift-XRT and Swift-BAT. The spectra were fitted utilizing physically motivated AGN models by Murphy & Yaqoob (2009) and Baloković et al. (2018) in order to investigate its true nature; i.e., either it is intrinsically an LLAGN, heavily obscured AGN, or both. Both best-fitted models indicate that the AGN in NGC 4117 is a CTAGN, with a measured column density of $\geqslant 10^{24}\,\mathrm{cm^{-2}}$. Despite that, in the spectra of the AGN, no iron line was found, possibly due to lack of X-ray data. So, more high quality data can help in confirming the presence of the iron line.

Based on our analysis, the 2–10 keV observed luminosity measured is $(1.42–1.46) \times 10^{39}\,\mathrm{erg\,s^{-1}}$ whereas the intrinsic luminosity is $(0.51–1.54) \times 10^{42}\,\mathrm{erg\,s^{-1}}$, which is approximately 600 times greater than the observed one. Even so, the intrinsic luminosity measured is comparable with that estimated by Terashima et al. (2000) using the ASCA data alone, but slightly higher than that estimated by Nucita et al. (2017) using XMM-Newton data. The discrepancies are likely due to the different data as well as models used to fit the spectra. Our result could be considered more reliable because of the utilization of broadband X-ray spectra, covering the energy band 0.5 to 195.0 keV.

The bolometric luminosity, L_{bol}, calculated for the AGN using the bolometric correction of AGN, $L_{\mathrm{bol}}/L_{2-10,\mathrm{int}} \approx 20$ (e.g., Vasudevan et al. 2010), is $(1.01–3.08) \times 10^{43}\,\mathrm{erg\,s^{-1}}$. This reveals that the AGN is a standard AGN, and not an LLAGN as suggested by past studies (e.g., Terashima et al. 2000; Nucita et al. 2017). Then, we determined the Eddington ratio of the AGN, λ_{Edd} ($L_{\mathrm{bol}}/L_{\mathrm{Edd}}$), using the calculated bolometric luminosity and the mass of the black hole estimated by Nucita et al. (2017); i.e., $M_{\mathrm{BH}} = 6.91 \times 10^5\ M_{\odot}$. We obtained a λ_{Edd} value of (0.11–0.32). This is significantly higher than the predicted value of 9.7×10^{-5} by Nucita et al. (2017) using XMM-Newton data alone. However, our Eddington ratio suggested that the AGN in NGC 4117 is undergoing a high accretion rate. For further validation, we compared NGC 4117 to other Swift-BAT AGNs ($z < 0.03$) from Koss et al. (2017) in Figure 3 and noticed that NGC 4117 is consistent with other AGNs. This high accretion rate of NGC 4117 could be the reason for the heavy obscuration in the AGN as the high radiation pressure from the accretion influences dust and gas cloud outflows around the source (Elitzur & Shlosman 2006; Fabian et al. 2006; Ricci et al. 2017b), which eventually causes obscuration. This supports previous studies that suggested accretion rate to be a factor for AGN obscuration (Treister et al. 2010; She et al. 2018).

Since X-ray radiation emitted by an AGN's core engine is absorbed through its torus, but also re-emitted in the mid-infrared band (López-Gonzaga 2016), we can use measurements from this band to determine the veracity of our X-ray findings. We calculated the AGN's 12 μm luminosity using data obtained by the Wide-field Infrared Survey Explorer (WISE) (Wright et al. 2010). The flux measured for the AGN at 12 μm is $2.65 \times 10^{-12}\,\mathrm{erg\,cm^{-2}\,s^{-1}}$, yielding a luminosity of $5.50 \times 10^{40}\,\mathrm{erg\,s^{-1}}$. We investigated whether the 2–10 keV X-ray luminosity measured in our best-fitted models agrees with this value using the X-ray:mid-infrared correlation (Asmus et al. 2015). According to the correlation demonstrated by Figure 4, the observed luminosity of NGC 4117 is below the relation, comparable to other genuine local CTAGNs from Gandhi et al. (2014), while the intrinsic luminosity is closer to NGC 4945. In that case, we also calculated the ratio of mid-infrared and X-ray by Asmus et al. (2015) and obtained a lower ratio of −1.27 compared to the average value of 0.39; however, it is quite similar to −2.15, the ratio measured for one of the CTAGNs (NGC 4945). According to Asmus et al. (2015), the low ratio obtained for NGC 4945 suggested that the AGN's mid-infrared emission may be influenced by unresolved

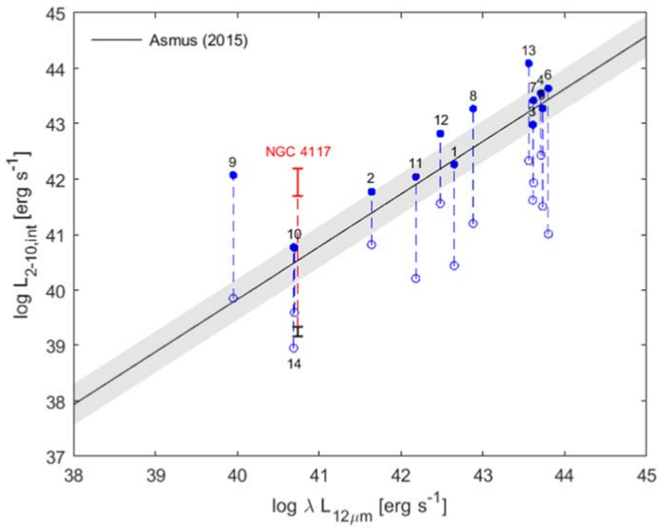

Figure 4. The plot of 2–10 keV intrinsic luminosity vs. 12 μm luminosity of NGC 4117 and local bona fide CTAGNs from Gandhi et al. (2014), adapted from Annuar et al. (2017). For NGC 4117, the 2–10 keV observed luminosity is indicated by a red solid mark, while the intrinsic luminosity by black solid marks. The relation of 2–10 keV luminosity vs. 12 μm luminosity from Asmus et al. (2015) is illustrated with the black solid line, whereas its intrinsic scatter with the shaded region. For the local bona fide CTAGNs (Gandhi et al. 2014), the blue open circles indicate the observed luminosity and the blue filled circles correspond to the intrinsic luminosity, with respect to the 12 μm luminosity, which is accessible in Asmus et al. (2015). The following are the plotted local CTAGNs, and if the X-ray data were not adopted from Asmus et al. (2015), the reference is indicated in parentheses: (1) Circinus; (2) ESO 5-G4 (3) ESO 138-G1; (4) Mrk 3; (5) NGC 424; (6) NGC 1068; (7) NGC 3281; (8) NGC 3393; (9) NGC 4945; (10) NGC 5194 (Terashima et al. 1998; Goulding et al. 2012); (11) NGC 5643 (Annuar et al. 2015); (12) NGC 5728; (13) NGC 6240; (14) NGC 1448 (Annuar et al. 2017).

circumnuclear star formation or possibly affected by poor intrinsic resolution of mid-infrared or X-ray emission. Therefore, we are expecting similar possible reasons for NGC 4117, despite that we also might need higher resolution mid-infrared and X-ray data to verify our findings.

High host galaxy inclination can potentially misidentify an AGN as Compton-thick because of the additional absorption column along our line-of-sight from the galaxy itself. However, Annuar et al. (2017) have shown that the host galaxy's inclination has no influence on the identification of CTAGN. Therefore, the host galaxy obscuration factor that could be caused by the galaxy's edge-on inclination angle should not affect our results. Data from a more sensitive high energy X-ray telescope, e.g., NuSTAR, are important to verify our findings, especially to really characterize the AGN broadband X-ray spectra in more detail, e.g., detect the narrow Fe Kα line associated with CTAGN. Further studies on NGC 4117 in different wavelengths such as optical and mid-infrared are also essential to observe the galaxy in greater detail.

Acknowledgments

We appreciate the support provided for this research from Fundamental Research Grant Scheme code FRGS/1/2019/STG02/UKM/02/7, which is funded by the Malaysian Ministry of Higher Education (MoHE). The all-sky hard X-ray survey of the Swift Observatory, having Burst Alert Telescope on board, operating at the 14–195 keV energy band allowed us to detect a buried AGN. Therefore, we would like to express our gratitude to the Swift Operations, Software and Calibrations teams for their assistance throughout this research. We are also grateful to Kyuseok Oh for providing processed Swift-BAT data. This study used data from XMM-Newton, one of the ESA science projects involving equipment and resources primarily sponsored by the ESA Member States and the National Aeronautics and Space Administration (NASA). The XMM software team provided the Software Analysis System (SAS) for reducing the XMM-Newton data. The NASA/IPAC Extragalactic Database (NED) was used in this study and is run by the Jet Propulsion Laboratory at the California Institute of Technology in collaboration with NASA.

References

Annuar, A., Alexander, D. M., Gandhi, P., et al. 2017, ApJ, 836, 165
Annuar, A., Alexander, D. M., Gandhi, P., et al. 2020, MNRAS, 497, 229
Annuar, A., Gandhi, P., Alexander, D. M., et al. 2015, ApJ, 815, 36
Antonucci, R. 1993, ARA&A, 31, 473
Arnaud, K. A. 1996, in ASP Conf. Ser. 101, Astronomical Data Analysis Software and Systems V, ed. G. H. Jacoby & J. Barnes (San Francisco, CA: ASP), 17
Asmus, D., Gandhi, P., Hönig, S. F., Smette, A., & Duschl, W. J. 2015, MNRAS, 454, 766
Baloković, M., Brightman, M., Harrison, F. A., et al. 2018, ApJ, 854, 42
Baumgartner, W. H., Tueller, J., Markwardt, C. B., et al. 2013, ApJS, 207, 19
Comastri, A., Gilli, R., Marconi, A., Risaliti, G., & Salvati, M. 2015, A&A, 574, L10
Diaz, Y., Arévalo, P., Hernández-García, L., et al. 2020, MNRAS, 496, 5399
Elitzur, M., & Shlosman, I. 2006, ApJL, 648, L101
Eracleous, M., Hwang, J. A., & Flohic, H. M. L. G. 2010, ApJS, 187, 135
Fabian, A. C., Celotti, A., & Erlund, M. C. 2006, MNRAS, 373, L16
Gandhi, P., Lansbury, G. B., Alexander, D. M., et al. 2014, ApJ, 792, 117
Gehrels, N., Chincarini, G., Giommi, P., et al. 2004, ApJ, 611, 1005
González-Martín, O., Masegosa, J., Hernán-Caballero, A., et al. 2017, ApJ, 841, 37
Goulding, A. D., Alexander, D. M., Bauer, F. E., et al. 2012, ApJ, 755, 5
Guainazzi, M., Mihara, T., Otani, C., & Matsuoka, M. 1996, PASJ, 48, 781
Imanishi, M., Dudley, C. C., Maiolino, R., et al. 2007, ApJS, 171, 72
Kalberla, P. M. W., Burton, W. B., Hartmann, D., et al. 2005, A&A, 440, 775
Koss, M., Trakhtenbrot, B., Ricci, C., et al. 2017, ApJ, 850, 74
Lambrides, E. L., Chiaberge, M., Heckman, T., et al. 2020, ApJ, 897, 160
López-Gonzaga, N. 2016, The structure of the dusty cores of active galactic nuclei, PhD thesis (Netherlands: Univ. Leiden)
Macchetto, F. D., & Chiaberge, M. 2007, Radiatively inefficient accretion disks in low-luminosity AGN?, in Proc. IAU, Vol. 238, ed. V. Karas & G. Matt (Cambridge: Cambridge Univ. Press), 273
Madsen, K. K., Harrison, F. A., Markwardt, C. B., et al. 2015, ApJS, 220, 8
Marchesi, S., Ajello, M., Marcotulli, L., et al. 2018, ApJ, 854, 49
Mason, R. E., Ramos Almeida, C., Levenson, N. A., Nemmen, R., & Alonso-Herrero, A. 2013, ApJ, 777, 164
Murphy, K. D., & Yaqoob, T. 2009, MNRAS, 397, 1549
Nucita, A. A., Manni, L., De Paolis, F., Giordano, M., & Ingrosso, G. 2017, ApJ, 837, 66
Oh, K., Koss, M., Markwardt, C. B., et al. 2018, ApJS, 235, 4
Oyaizu, H., Lima, M., Cunha, C. E., et al. 2008, ApJ, 674, 768
Panessa, F., Bassani, L., Cappi, M., et al. 2006, A&A, 455, 173
Ricci, C., Bauer, F. E., Treister, E., et al. 2016, ApJ, 819, 4
Ricci, C., Trakhtenbrot, B., Koss, M. J., et al. 2017a, ApJS, 233, 17
Ricci, C., Trakhtenbrot, B., Koss, M. J., et al. 2017b, Natur, 549, 488
Shakura, N. I., & Sunyaev, R. A. 1973, A&A, 24, 337
She, R., Ho, L. C., Feng, H., & Cui, C. 2018, ApJ, 859, 152
Terashima, Y., Ho, L. C., Ptak, A. F., et al. 2000, ApJ, 533, 729
Terashima, Y., Iyomoto, N., Ho, L. C., & Ptak, A. F. 2002, ApJS, 139, 1
Terashima, Y., Ptak, A., Fujimoto, R., et al. 1998, ApJ, 496, 210
Torres-Albà, N., Marchesi, S., Zhao, X., et al. 2021, ApJ, 922, 252
Traina, A., Marchesi, S., Vignali, C., et al. 2021, ApJ, 922, 159
Treister, E., Schawinski, K., Urry, C. M., & Simmons, B. D. 2012, ApJL, 758, L39
Treister, E., Urry, C. M., Schawinski, K., Cardamone, C. N., & Sanders, D. B. 2010, ApJL, 722, L238
Ueda, Y., Akiyama, M., Hasinger, G., Miyaji, T., & Watson, M. G. 2014, ApJ, 786, 104
Urry, C. M., & Padovani, P. 1995, PASP, 107, 803
Vasudevan, R. V., Fabian, A. C., Gandhi, P., Winter, L. M., & Mushotzky, R. F. 2010, MNRAS, 402, 1081
Verheijen, M. A. W., & Sancisi, R. 2001, A&A, 370, 765
Wright, E. L., Eisenhardt, P. R. M., Mainzer, A. K., et al. 2010, AJ, 140, 1868
Yaqoob, T. 2012, MNRAS, 423, 3360
Younes, G., Porquet, D., Sabra, B., & Reeves, J. N. 2011, A&A, 530, A149
Yuan, F., & Narayan, R. 2014, ARA&A, 52, 529